HGF has not only angiogenic but also cardioprotective effects, including antiapoptotic, mitogenic, and antifibrotic activities.[26,27] *HGF* gene transfer into the myocardium improves myocardial function and geometry.[28] In particular, the antifibrotic effects of HGF through inhibition of transforming growth factor-β expression is beneficial for heart failure. Cultured MSCs secreted a large amount of HGF. In vivo, transplantation of MSCs slightly increased plasma HGF in rats. It significantly attenuated the development of myocardial fibrosis in a rat model of DCM. These results suggest that MSC-derived HGF may contribute to improvements in cardiac function partly through its antifibrotic effects.

MSCs also produced AM, a potent vasodilator and cardioprotective peptide.[29] We have shown that AM prevents cardiomyocyte apoptosis through the phosphatidylinositol 3-kinase/Akt–dependent pathway[16] and that it has potent angiogenic effects.[30] AM inhibits proliferation of cardiac fibroblasts through the cAMP-dependent pathway.[31] Administration of AM inhibits LV remodeling and improves cardiac function in heart failure.[32–34] In the present study, cultured MSCs secreted a large amount of AM in vitro. In vivo, transplantation of MSCs markedly increased plasma AM level. Taken together, these findings suggest that MSCs may exert their cardioprotective effects through AM-mediated paracrine regulation.

IGF-1, a growth hormone mediator, plays an important role in myocardial and skeletal muscle growth.[35,36] Administration of IGF-1 improves cardiac function after myocardial infarction through enhancement of myocardial growth.[37] Its protective and antiapoptotic properties have been demonstrated in different models of myocardial ischemia.[38] Furthermore, IGF-1 exerts Ca^{2+}-dependent, positive inotropic effects through a phosphatidylinositol 3-kinase–dependent pathway.[39] Interestingly, the present study demonstrated that MSCs secreted significant amounts of IGF-1 in vitro, 10-fold greater than MNCs. These findings raise the possibility that MSC-derived IGF-1 may participate in myocardial growth and enhancement of myocardial contractility in a rat model of DCM.

MMPs also play a crucial role in extracellular remodeling in heart failure.[40] In fact, pharmacological inhibition of MMP activities prevents progressive LV remodeling in an animal model of heart failure.[41] In the present study, cardiac MMP-2 and MMP-9 were increased in rats with DCM, which is consistent with recent findings in patients with heart failure.[40,42] Interestingly, MSC transplantation attenuated the increases in cardiac MMP-2 and MMP-9 in a rat model of DCM. Although the underlying mechanisms remain unclear, MSC transplantation may influence extracellular remodeling in heart failure.

The present study has some limitations. First, immunohistochemical evidence suggests differentiation of MSCs into cardiomyocytes, vascular endothelial cells, and smooth muscle cells. However, further studies are necessary to convincingly demonstrate differentiation of MSCs into a specific cell type. Second, the model of DCM used in this study was an injury model, and the effects of treatment may be related to attenuation of the injury rather than to the established cardiomyopathy. Nonetheless, the experiment was performed 5 to 9 weeks after myosin injection, by which time inflammatory changes were hardly observed and had been replaced by fibrosis.[43]

Conclusions

MSC transplantation improved cardiac function in a rat model of DCM, possibly through induction of myogenesis and angiogenesis, as well as by inhibition of myocardial fibrosis. The beneficial effects of MSCs may be mediated at least in part by their differentiation into cardiomyocytes and vascular cells and by their ability to supply large amounts of angiogenic, antiapoptotic, and mitogenic factors. Thus, MSC transplantation has potential as a new therapeutic strategy for the treatment of DCM.

Acknowledgments

This work was supported by research grants for cardiovascular disease (16C-6) and Human Genome Tissue Engineering 009 from the Ministry of Health, Labor and Welfare; the Industrial Technology Research Grant Program in '03 from the New Energy and Industrial Technology Development Organization of Japan; a research grant from the Japan Cardiôvascular Research Foundation; and Promotion of Fundamental Studies in Health Science of the Organization for Pharmaceutical Safety and Research of Japan.

References

1. Cohn JN. The management of chronic heart failure. *N Engl J Med.* 1996;335:490–498.
2. Dec GW, Fuster V. Idiopathic dilated cardiomyopathy. *N Engl J Med.* 1994;331:1564–1575.
3. Beltrami AP, Urbanek K, Kajstura J, Yan SM, Finato N, Bussani R, Nadal-Ginard B, Silvestri F, Leri A, Beltrami CA, Anversa P. Evidence that human cardiac myocytes divide after myocardial infarction. *N Engl J Med.* 2001;344:1750–1757.
4. Pittenger MF, Mackay AM, Beck SC, Jaiswal RK, Douglas R, Mosca JD, Moorman MA, Simonetti DW, Craig S, Marshak DR. Multilineage potential of adult human mesenchymal stem cells. *Science.* 1999;284:143–147.
5. Reyes M, Dudek A, Jahagirdar B, Koodie L, Marker PH, Verfaillie CM. Origin of endothelial progenitors in human postnatal bone marrow. *J Clin Invest.* 2002;109:337–346.
6. Toma C, Pittenger MF, Cahill KS, Byrne BJ, Kessler PD. Human mesenchymal stem cells differentiate to a cardiomyocyte phenotype in the adult murine heart. *Circulation.* 2002;105:93–98.
7. Mangi AA, Noiseux N, Kong D, He H, Rezvani M, Ingwall JS, Dzau VJ. Mesenchymal stem cells modified with Akt prevent remodeling and restore performance of infarcted hearts. *Nat Med.* 2003;9:1195–1201.
8. Makino S, Fukuda K, Miyoshi S, Konishi F, Kodama H, Pan J, Sano M, Takahashi T, Hori S, Abe H, Hata J, Umezawa A, Ogawa S. Cardiomyocytes can be generated from marrow stromal cells in vitro. *J Clin Invest.* 1999;103:697–705.
9. Shake JG, Gruber PJ, Baumgartner WA, Senechal G, Meyers J, Redmond JM, Pittenger MF, Martin BJ. Mesenchymal stem cell implantation in a swine myocardial infarct model: engraftment and functional effects. *Ann Thorac Surg.* 2002;73:1919–1925.
10. Al-Khaldi A, Al-Sabti H, Galipeau J, Lachapelle K. Therapeutic angiogenesis using autologous bone marrow stromal cells: improved blood flow in a chronic limb ischemia model. *Ann Thorac Surg.* 2003;75:204–209.
11. Al-Khaldi A, Eliopoulos N, Martineau D, Lejeune L, Lachapelle K, Galipeau J. Postnatal bone marrow stromal cells elicit a potent VEGF-dependent neoangiogenic response in vivo. *Gene Ther.* 2003;10:621–629.
12. Parodi O, De Maria R, Oltrona L, Testa R, Sambuceti G, Roghi A, Merli M, Belingheri L, Accinni R, Spinelli F, Pellegrini A, Baroldi G. Myocardial blood flow distribution in patients with ischemic heart disease or dilated cardiomyopathy undergoing heart transplantation. *Circulation.* 1993;88:509–522.
13. Kodama M, Zhang S, Hanawa H, Saeki M, Inomata T, Suzuki K, Koyama S, Shibata A. Effects of 15-deoxyspergualin on experimental autoimmune giant cell myocarditis of the rat. *Circulation.* 1995;91:1116–1122.
14. Watanabe K, Ohta Y, Nakazawa M, Higuchi H, Hasegawa G, Naito M, Fuse K, Ito M, Hirono S, Tanabe N, Hanawa H, Kato K, Kodama M, Aizawa Y. Low dose carvedilol inhibits progression of heart failure in rats with dilated cardiomyopathy. *Br J Pharmacol.* 2000;130:1489–1495.

15. Nagaya N, Uematsu M, Kojima M, Ikeda Y, Yoshihara F, Shimizu W, Hosoda H, Hirota Y, Ishida H, Mori H, Kangawa K. Chronic administration of ghrelin improves left ventricular dysfunction and attenuates development of cardiac cachexia in rats with heart failure. *Circulation*. 2001;104:1430–1435.
16. Okumura H, Nagaya N, Itoh T, Okano I, Hino J, Mori K, Tsukamoto Y, Ishibashi-Ueda H, Miwa S, Tambara K, Toyokuni S, Yutani C, Kangawa K. Adrenomedullin infusion attenuates myocardial ischemia/reperfusion injury through the phosphatidylinositol 3-kinase/Akt-dependent pathway. *Circulation*. 2004;109:242–248.
17. Messina LM, Podrazik RM, Whitehill TA, Ekhterae D, Brothers TE, Wilson JM, Burkel WE, Stanley JC. Adhesion and incorporation of lacZ-transduced endothelial cells into the intact capillary wall in the rat. *Proc Natl Acad Sci U S A*. 1992;89:12018–12022.
18. Harada M, Itoh H, Nakagawa O, Ogawa Y, Miyamoto Y, Kuwahara K, Ogawa E, Igaki T, Yamashita J, Masuda I, Yoshimasa T, Tanaka I, Saito Y, Nakao K. Significance of ventricular myocytes and nonmyocytes interaction during cardiocyte hypertrophy: evidence for endothelin-1 as a paracrine hypertrophic factor from cardiac nonmyocytes. *Circulation*. 1997;96:3737–3744.
19. Ohta H, Tsuji T, Asai S, Sasakura K, Teraoka H, Kitamura K, Kangawa K. A simple immunoradiometric assay for measuring the entire molecules of adrenomedullin in human plasma. *Clin Chim Acta*. 1999;287:B131–B143.
20. Murohara T, Ikeda H, Duan J, Shintani S, Sasaki K, Eguchi H, Onitsuka I, Matsui K, Imaizumi T. Transplanted cord blood-derived endothelial precursor cells augment postnatal neovascularization. *J Clin Invest*. 2000; 105:1527–1536.
21. Tateishi-Yuyama E, Matsubara H, Murohara T, Ikeda U, Shintani S, Masaki H, Amano K, Kishimoto Y, Yoshimoto K, Akashi H, Shimada K, Iwasaka T, Imaizumi T. Therapeutic Angiogenesis using Cell Transplantation (TACT) Study Investigators. Therapeutic angiogenesis for patients with limb ischaemia by autologous transplantation of bone-marrow cells: a pilot study and a randomised controlled trial. *Lancet*. 2002;360:427–435.
22. Tse HF, Kwong YL, Chan JK, Lo G, Ho CL, Lau CP. Angiogenesis in ischaemic myocardium by intramyocardial autologous bone marrow mononuclear cell implantation. *Lancet*. 2003;4:47–49.
23. Min JY, Sullivan MF, Yang Y, Zhang JP, Converso KL, Morgan JP, Xiao YF. Significant improvement of heart function by cotransplantation of human mesenchymal stem cells and fetal cardiomyocytes in postinfarcted pigs. *Ann Thorac Surg*. 2002;74:1568–1575.
24. Kamihata H, Matsubara H, Nishiue T, Fujiyama S, Tsutsumi Y, Ozono R, Masaki H, Mori Y, Iba O, Tateishi E, Kosaki A, Shintani S, Murohara T, Imaizumi T, Iwasaka T. Implantation of bone marrow mononuclear cells into ischemic myocardium enhances collateral perfusion and regional function via side supply of angioblasts, angiogenic ligands, and cytokines. *Circulation*. 2001;104:1046–1052.
25. Kinnaird T, Stabile E, Burnett MS, Lee CW, Barr S, Fuchs S, Epstein SE. Marrow-derived stromal cells express genes encoding a broad spectrum of arteriogenic cytokines and promote in vitro and in vivo arteriogenesis through paracrine mechanisms. *Circ Res*. 2004;94:678–685.
26. Nakamura T, Nishizawa T, Hagiya M, Seki T, Shimonishi M, Sugimura A, Tashiro K, Shimizu S. Molecular cloning and expression of human hepatocyte growth factor. *Nature*. 1989;342:440–443.
27. Nakamura T, Mizuno S, Matsumoto K, Sawa Y, Matsuda H, Nakamura T. Myocardial protection from ischemia/reperfusion injury by endogenous and exogenous HGF. *J Clin Invest*. 2000;106:1511–1519.
28. Li Y, Takemura G, Kosai K, Yuge K, Nagano S, Esaki M, Goto K, Takahashi T, Hayakawa K, Koda M, Kawase Y, Maruyama R, Okada H, Minatoguchi S, Mizuguchi H, Fujiwara T, Fujiwara H. Postinfarction treatment with an adenoviral vector expressing hepatocyte growth factor relieves chronic left ventricular remodeling and dysfunction in mice. *Circulation*. 2003;107:2499–2506.
29. Kitamura K, Kangawa K, Kawamoto M, Ichiki Y, Nakamura S, Matsuo H, Eto T. Adrenomedullin: a novel hypotensive peptide isolated from human pheochromocytoma. *Biochem Biophys Res Commun*. 1993;192:553–560.
30. Tokunaga N, Nagaya N, Shirai M, Tanaka E, Ishibashi-Ueda H, Harada-Shiba M, Kanda M, Ito T, Shimizu W, Tabata Y, Uematsu M, Nishigami K, Sano S, Kangawa K, Mori H. Adrenomedullin gene transfer induces therapeutic angiogenesis in a rabbit model of chronic hind limb ischemia: benefits of a novel nonviral vector, gelatin. *Circulation*. 2004;109:526–531.
31. Tsuruda T, Kato J, Kitamura K, Kawamoto M, Kuwasako K, Imamura T, Koiwaya Y, Tsuji T, Kangawa K, Eto T. An autocrine or a paracrine role of adrenomedullin in modulating cardiac fibroblast growth. *Cardiovasc Res*. 1999;43:958–967.
32. Nishikimi T, Yoshihara F, Horinaka S, Kobayashi N, Mori Y, Tadokoro K, Akimoto K, Minamino N, Kangawa K, Matsuoka H. Chronic administration of adrenomedullin attenuates transition from left ventricular hypertrophy to heart failure in rats. *Hypertension*. 2003;42:1034–1041.
33. Nakamura R, Kato J, Kitamura K, Onitsuka H, Imamura T, Cao Y, Marutsuka K, Asada Y, Kangawa K, Eto T. Adrenomedullin administration immediately after myocardial infarction ameliorates progression of heart failure in rats. *Circulation*. 2004;110:426–431.
34. Nagaya N, Satoh T, Nishikimi T, Uematsu M, Furuichi S, Sakamaki F, Oya H, Kyotani S, Nakanishi N, Goto Y, Masuda Y, Miyatake K, Kangawa K. Hemodynamic, renal, and hormonal effects of adrenomedullin infusion in patients with congestive heart failure. *Circulation*. 2000;101:498–503.
35. Fuller J, Mynett JR, Sugden PH. Stimulation of cardiac protein synthesis by insulin-like growth factors. *Biochem J*. 1992;282:85–90.
36. Florini JR, Ewton DZ, Coolican SA. Growth hormone and the insulin-like growth factor system in myogenesis. *Endocr Rev*. 1996;17:481–517.
37. Cittadini A, Stromer H, Katz SE, Clark R, Moses AC, Morgan JP, Douglas PS. Differential cardiac effects of growth hormone and insulin-like growth factor-1 in the rat: a combined in vivo and in vitro evaluation. *Circulation*. 1996;93:800–809.
38. Li Q, Li B, Wang X, Leri A, Jana KP, Liu Y, Kajstura J, Baserga R, Anversa P. Overexpression of insulin-like growth factor-1 in mice protects from myocyte death after infarction, attenuating ventricular dilation, wall stress, and cardiac hypertrophy. *J Clin Invest*. 1997;100:1991–1999.
39. von Lewinski D, Voss K, Hulsmann S, Kogler H, Pieske B. Insulin-like growth factor-1 exerts Ca^{2+}-dependent positive inotropic effects in failing human myocardium. *Circ Res*. 2003;92:169–176.
40. Thomas CV, Coker ML, Zellner JL, Handy JR, Crumbley AJ 3rd, Spinale FG. Increased matrix metalloproteinase activity and selective upregulation in LV myocardium from patients with end-stage dilated cardiomyopathy. *Circulation*. 1998;97:1708–1715.
41. Spinale FG, Coker ML, Krombach SR, Mukherjee R, Hallak H, Houck WV, Clair MJ, Kribbs SB, Johnson LL, Peterson JT, Zile MR. Matrix metalloproteinase inhibition during the development of congestive heart failure: effects on left ventricular dimensions and function. *Circ Res*. 1999;85:364–376.
42. Spinale FG, Coker ML, Heung LJ, Bond BR, Gunasinghe HR, Etoh T, Goldberg AT, Zellner JL, Crumbley AJ. A matrix metalloproteinase induction/activation system exists in the human left ventricular myocardium and is upregulated in heart failure. *Circulation*. 2000;102:1944–1949.
43. Kodama M, Matsumoto Y, Fujiwara M, Zhang SS, Hanawa H, Itoh E, Tsuda T, Izumi T, Shibata A. Characteristics of giant cells and factors related to the formation of giant cells in myocarditis. *Circ Res*. 1991;69:1042–1050.

CLINICAL PERSPECTIVE

Transplantation of stem or progenitor cells has the potential to improve and restore cardiac function. To date, experimenters investigating the possible therapeutic effects of stem cells in the heart have used models of infarction, and little information is available about the therapeutic potential of cell transplantation for heart failure due to dilated cardiomyopathy. In the present study, we demonstrated that transplantation of stem cells improved cardiac function in a model of myocarditis. We found evidence that stem cells may work to improve heart function by both myogenesis and angiogenesis while inhibiting myocardial fibrosis. Based on our data, part of the mechanism for this improvement may occur through the action of stem cells as a source of growth factors and cytokines in the heart. This study supports the overall notion that mesenchymal stem cells transplanted into the failing heart have potential as a new therapeutic strategy for the treatment of dilated cardiomyopathy.

Available online at www.sciencedirect.com
SCIENCE DIRECT®
Neuroscience Letters 388 (2005) 61–64
Neuroscience Letters
www.elsevier.com/locate/neulet

Contribution of catechol *O*-methyltransferase to the removal of accumulated interstitial catecholamines evoked by myocardial ischemia

Yosuke Kuroko [a], Takafumi Fujii [a], Toji Yamazaki [b,*], Tsuyoshi Akiyama [b], Kozo Ishino [a], Shunji Sano [a], Hidezo Mori [b]

[a] *Department of Cardiovascular Surgery, Okayama University Graduate School of Medicine and Dentistry, Okayama 700-8558 Japan*
[b] *Department of Cardiac Physiology, National Cardiovascular Center Research Institute, 5-7-1 Fujishiro-dai, Suitâ, Osaka 565-8565 Japan*

Received 7 May 2005; received in revised form 15 June 2005; accepted 16 June 2005

Abstract

Catechol *O*-methyltransferase (COMT) plays an important role for clearance of high catecholamine levels. Although myocardial ischemia evokes similar excessive catecholamine accumulation, it is uncertain whether COMT activity is involved in the removal of accumulated catecholamines evoked by myocardial ischemia. We examined how COMT activity affects myocardial catecholamine levels during myocardial ischemia and reperfusion. We implanted a dialysis probe into the left ventricular myocardial free wall and measured dialysate catecholamines levels in anesthetized rabbits. Dialysate catecholamine levels served as an index of myocardial interstitial catecholamine levels. We introduced myocardial ischemia by 60 min occlusion of the main coronary artery. The ischemia-induced dialysate catecholamines levels were compared with and without the pretreatment with entacapone (COMT inhibitor, 10 mg/kg, i.p.). Acute myocardial ischemia progressively increased dialysate catecholamine levels. Acute myocardial ischemia increased dialysate norepinephrine (NE) levels (20,453 ± 7186 pg/ml), epinephrine (EPI) levels (1724 ± 706 pg/ml), and dopamine (DA) levels (1807 ± 800 pg/ml) at the last 15 min of coronary occlusion. Inhibition of COMT activity by entacapone augmented the ischemia-induced NE levels (54,306 ± 6618 pg/ml), EPI levels (2681 ± 567 pg/ml), and DA (3551 ± 710 pg/ml) levels at the last 15 min of coronary occlusion. Myocardial ischemia evoked NE, EPI, and DA accumulation in the myocardial interstitial space. The inhibition of COMT activity augmented these increments in NE, EPI, and DA. These data suggest that cardiac COMT activity influences on the removal of accumulated catecholamine during myocardial ischemia.

Keywords: Catecholamine; Microdialysis; Myocardial infarction; Heart; Catechol *O*-methyltransferase

Myocardial ischemia evokes an excessive norepinephrine (NE) accumulation in the myocardial interstitial space [2,15]. Interstitial NE is largely removed by NE transport into the sympathetic nerve endings and metabolized to dihydroxyphenylglycol (DHPG) via monoamine oxidase (MAO) [6,22]. The remainder spills over into the coronary sinus [6]. However, during myocardial ischemia, two important NE removing systems are impaired. Myocardial ischemia reduces coronary flow, which abolishes NE spillover. Furthermore, membrane NE transport is dependent on the Na^+ gradient between the extracellular and intracellular spaces. During ischemia, NE uptake is blocked and outward NE transport through the uptake$_1$ carrier is induced by the reduced Na^+ gradient [17]. Thus, production of DHPG via MAO is inhibited by myocardial ischemia [1]. Up to now, little has been known about the role of catechol *O*-methyltransferase (COMT) in the removal of interstitial NE. Catechol *O*-methyltransferase has been believed to be operative only at high concentrations of NE via NE infusion [12]. An excessive NE accumulation in the myocardial ischemia was similar to NE levels in

* Corresponding author. Tel.: +81 6 6833 5012x2379; fax: +81 6 6872 8092.
E-mail address: yamazaki@ri.ncvc.go.jp (T. Yamazaki).

0304-3940/$ – see front matter © 2005 Elsevier Ireland Ltd. All rights reserved.
doi:10.1016/j.neulet.2005.06.031

intravenous NE infusion. Therefore, this NE removal system may be the sole mechanism that decreases myocardial interstitial NE.

Recent study has demonstrated that myocardial ischemia is associated with a pronounced increase in the concentration of endogenous NE, epinephrine (EPI), dopamine (DA) in the myocardial interstitial space [14]. These accumulated catecholamines may be a candidate of substrate of COMT. However, in most experiments on COMT activity, isoprenaline was used as the substrate of COMT [11,19] since it is not a substrate for neuronal uptake and MAO activity. Furthermore, data on isolated perfused lungs suggest that the affinity of COMT activity for *O*-methylation differed among the three amines [3]. It is uncertain whether COMT activity is involved in the removal of accumulated interstitial catecholamines evoked by myocardial ischemia.

In the present study, the possibility that the concentration of these three catecholamines in the myocardial interstitial space was affected by COMT activity was examined in anesthetized myocardial ischemic rabbits. With the use of dialysis technique, a dialysis probe was implanted into the left ventricle free wall perfused by the main branch of left circumflex coronary artery (LCX) to measure myocardial interstitial catecholamines levels in the ischemic region and dialysate catecholamines levels were compared in the absence and presence of COMT inhibitor.

Animal care proceeded in strict accordance with the *Guide for the Care and Use of Laboratory Animals* published by the US National Institutes of Health (NIH Publication No. 85-23, revised 1996). Adult male Japanese white rabbits (2.5–3.2 kg) were anesthetized with pentobarbital sodium (30–35 mg/kg i.v.). The level of anesthesia was maintained with a continuous intravenous infusion of pentobarbital sodium (1–2 mg/kg/h). The rabbits were intubated and ventilated with room air mixed with oxygen. Heart rate, arterial pressure, and electrocardiogram were simultaneously monitored with a data recorder. The fifth or sixth rib on the left side was partially removed to expose the heart. A 4–0 silk suture was passed around the main branch of LCX, to act as the occluder for later coronary occlusion. With a fine guiding needle, a dialysis probe was implanted in the region perfused by LCX of the left ventricular wall. Judging from changes in the color of the ventricular wall during a brief coronary occlusion, the dialysis probe was located in the midst of the ischemic region. Heparin sodium (100 IU/Kg) was administered intravenously to prevent blood coagulation.

The dialysate NE, EPI, and DA levels were measured as an index of myocardial interstitial NE, EPI, and DA levels, respectively. A dialysis fiber (8 mm length, 0.31 mm o.d., and 0.20 mm i.d.; PAN-1200 50,000 molecular weight cutoff, Asahi Chemical Japan) was glued at both ends of a polyethylene tube. The dialysis probe was perfused with Ringer's solution at a perfusion speed of 2 μl/min. Dialysate NE level was measured by the first HPLC after removing interfering compounds by the alumina procedure [23]. Dialysate EPI and DA levels were measured by direct injection into the second HPLC [18].

After control sampling, we occluded the main branch of LCX for 60 min and then released the occluder. The 15-min dialysate samples were collected before, during and after 60 min LCX occlusion. In vehicle group, we administered saline intraperitoneally as vehicle 120 min before control sampling. After control sampling, we observed the time course of dialysate NE, EPI, and DA levels from the ischemic region during 60 min of coronary occlusion and 15 min of reperfusion. To elucidate the role of COMT activity in the ischemia-induced changes in myocardial interstitial NE EPI, and DA levels, we compared dialysate NE, EPI, and DA levels in the ischemic region with those levels after injection of COMT inhibitor. We administered intraperitoneally the COMT inhibitor entacapone (10 mg/kg; Orion-Pharma, Espoo, Finland) 120 min before control sampling. Entacapone was dissolved in phosphate buffered saline, the pH of the solution was adjusted to 7.4, and the dose of entacapone was determined based on the dose used in the earlier preliminary experiments [7,8].

Changes in the dialysate NE levels in the vehicle and the pretreatment with entacapone are shown in Fig. 1. In the vehicle group, dialysate NE level averaged from six rabbits was 52 ± 12 pg/ml in the control. During 60 min coronary occlusion, dialysate NE levels markedly increased. The dialysate NE levels reached up to 400 times the control levels during the last 15 min of 60 min coronary occlusion. After release of the occluder, dialysate NE levels rapidly decreased to 3473 ± 735 pg/ml, although their levels were higher than those in the control. In the presence of entacapone, dialysate NE levels also markedly increased during 60 min coronary occlusion. The dialysate NE levels reached up to 1000 times the control levels during the last 15 min of 60 min coronary occlusion. These increases in dialysate NE levels at 15–60 min of coronary occlusion were significantly enhanced by entacapone whereas entacapone did not change dialysate NE levels in the control (51 ± 16 pg/ml) or at 0–15 min of

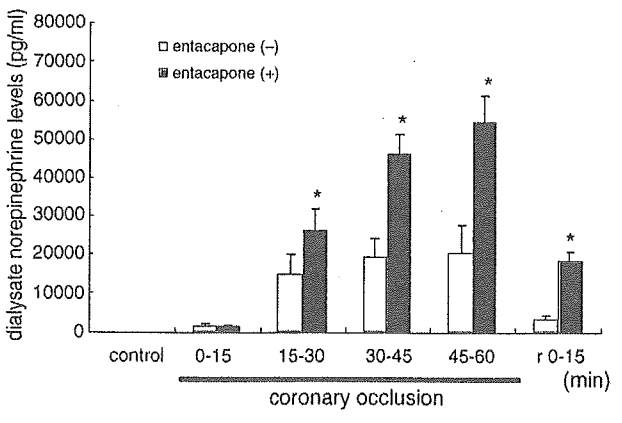

Fig. 1. Dialysate norepinephrine levels before, during and after 60 min-coronary occlusion. Values are mean ± S.E. ($n = 6$). $^{*}P < 0.05$ vs. concurrent value of vehicle group.

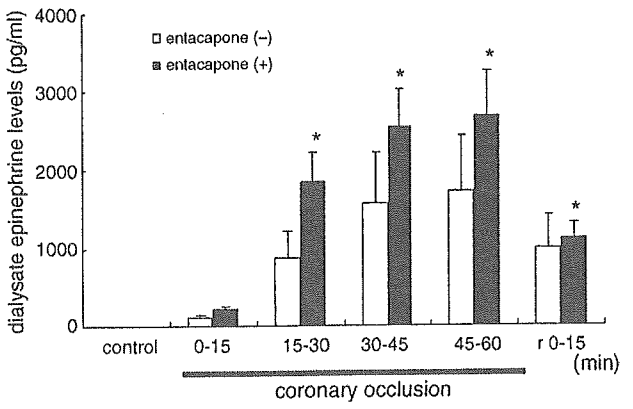

Fig. 2. Dialysate epinephrine levels before, during and after 60 min-coronary occlusion. Values are mean ± S.E. ($n = 6$). $^{*}P < 0.05$ vs. concurrent value of vehicle group.

coronary occlusion. Dialysate NE levels decreased by reperfusion, but remained higher than those in vehicle group. Thus, COMT activity for NE removal was operative in ischemic and reperfusion periods. Entacapone augmented peak NE levels to 160% of vehicle group.

Dialysate EPI levels were below the detectable level in the control. After coronary occlusion, dialysate EPI levels gradually increased and reached 1724 ± 706 pg/ml at 45–60 min of occlusion (Fig. 2). Peak EPI levels during the ischemia were one-twentieth of NE levels during the ischemic period. In the presence of entacapone, dialysate EPI levels were below the detectable level in the control. Dialysate EPI levels gradually increased during coronary occlusion and reached 2681 ± 567 pg/ml at 45–60 min of occlusion. In the presence of entacapone, dialysate EPI levels at 15–60 min of the ischemia were higher than those in the vehicle group. Entacapone augmented peak EPI levels by 50% of vehicle group.

Dialysate DA levels were below the detectable level in the control and at 0–15 min of ischemia. After 15 min of occlusion, dialysate DA levels gradually increased and reached 1807 ± 800 pg/ml at 45–60 min of occlusion (Fig. 3). Peak DA levels during the ischemia were one-twentieth of NE

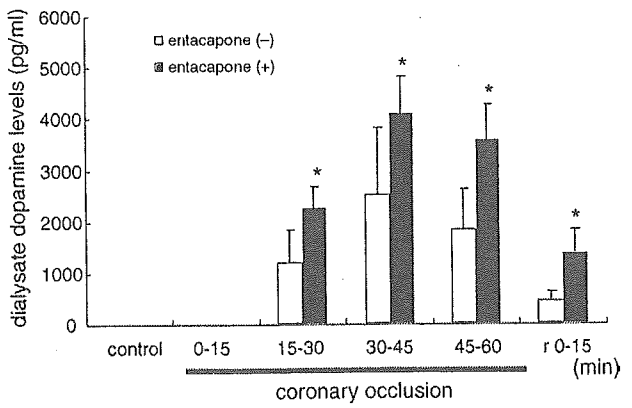

Fig. 3. Dialysate dopamine levels before, during and after 60 min-coronary occlusion. Values are mean ± S.E. ($n = 6$). $^{*}P < 0.05$ vs. concurrent value of vehicle group.

levels during the ischemia. In the presence of entacapone, dialysate DA levels were below the detectable level in the control and at 0–15 min of the occlusion. Dialysate DA levels gradually increased during 15–60 min of the ischemia and reached 3351 ± 710 pg/ml at 45–60 min of occlusion. In the presence of entacapone, dialysate DA levels at 15–60 min of the ischemia were higher than those in the vehicle group. Entacapone augmented peak DA levels by 100% of vehicle group.

Myocardial ischemia induced a progressive increase of interstitial catecholamines. The rank order of the amount of catecholamine release was NE much greater than EPI or DA, with this rank order remaining unchanged before, during and after myocardial ischemia. These findings are in line with those reported by Lameris et al. [14] studied the time course of myocardial interstitial catecholamine levels during myocardial ischemia. The measurement of overall content in the left ventricle free wall was performed in dogs [13] and the in vitro ratio of EPI/NE or DA/NE was similar to our result. Therefore, the rank order may reflect the ratio of overall catecholamine content in the left ventricle free wall.

In the resting state and early period (0–15 min) of ischemia, COMT does not appear to contribute to the removal of myocardial interstitial catecholamine levels. In the mid-late period of ischemia, COMT contributes to the inactivation of high myocardial interstitial catecholamine levels evoked by ischemia. The rank order of the amount of neurotransmitter release was NE much greater than EPI or DA. From percentage increase of catecholamine by entacapone, the rank order of COMT activity for removal of catecholamines was considered to be NE greater than DA greater than EPI. On the other hand, when catecholamines were infused in the isolated rat heart, the metabolism of the catecholamines by COMT differs: DA = NE less than EPI [9]. These data suggest that contribution of COMT to removal of accumulated catecholamines depends on the types of amines and the amount of accumulated catecholamine. In the absence of catecholamine spill over and MAO activity, COMT might constitutes one of major pathways of catecholamine metabolism in ischemic heart. Alternatively all three catecholamines are taken up and then metabolized by COMT at the extraneuronal tissues [4,10]. Uptake and *O*-methylation may handle three catecholamines in a different manner.

Up to now, little has been known about the role of cardiac COMT activity in the removal of accumulated interstitial catecholamine. In the isolated perfused rat, Carlsson et al. [5], demonstrated that marked NE release was paralleled by an increasing extraneuronal inactivation of released NE. Accumulated catecholamine in myocardial interstitial space is involved in the pathophysiology of ischemic heart disease [16,21]. Therefore, these data suggest that inhibition of COMT activity deteriorates myocardial ischemic injury via enhanced catecholamine accumulation. In contrast to this hypothesis, Valenza et al. [20], demonstrated that the inhibition of COMT (by nitecapone) improved the mechanical function of the heart during ischemia-reperfusion injury. In

the present study, we did not measure myocardial contractile function or biochemical markers. Future work should concentrate on these aspects of COMT action during myocardial ischemia.

Acknowledgement

This work was supported by Grands-in-Aid for scientific research (15590787) from the Ministry of Education, Culture, Sports, Science and Technology. The authors thank Orion-Pharma (Espoo, Finland) for the supply of entacapone.

References

[1] T. Akiyama, T. Yamazaki, Myocardial interstitial norepinephrine and dihydroxyphenylglycol levels during ischemia and reperfusion, Cardiovasc. Res. 49 (2001) 78–85.
[2] T. Akiyama, T. Yamazaki, I. Ninomiya, Differential regional responses of myocardial interstitial noradrenaline levels to coronary occlusion, Cardiovasc. Res. 27 (1993) 817–822.
[3] L.J. Bryan-Lluka, S.R. O'Donnell, Dopamine and adrenaline, but not isoprenaline, are substrates for uptake and metabolism in isolated perfused lungs of rats, Naunyn Schmiedebergs Arch. Pharmacol. 346 (1992) 20–26.
[4] C. Burgdorf, A. Dendorfer, T. Kurz, E. Schömig, I. Stolting, F. Schutte, G. Richardt, Role of neuronal KATP channels and extraneuronal monoamine transported on norepinephrine overflow in a model of myocardial low flow ischemia, J. Pharmacol. Exp. Ther. 309 (2004) 42–48.
[5] L. Carlsson, T. Abrahamsson, O. Almgren, Release of noradrenaline in myocardial ischemia-importance of local inactivation by neuronal and extraneuronal mechanisms, J. Cardiovasc Pharmacol. 8 (1986) 545–553.
[6] G. Eisenhofer, J.J. Smolich, H.S. Cox, M.D. Esler, Neuronal reuptake of norepinephrine and production of dihydroxyphenylglycol by cardiac sympathetic nerve in the anesthetized dog, Circulation 84 (1991) 1354–1363.
[7] T. Fujii, T. Yamazaki, T. Akiyama, S. Sano, H. Mori, In vivo assessment of catechol *O*-methyltransferase activity in rabbit skeletal muscle, Auton. Neurosci. 111 (2004) 140–143.
[8] T. Fujii, T. Yamazaki, T. Akiyama, S. Sano, H. Mori, Extraneuronal enzymatic degradation of myocardial norepinephrine in the ischemic region, Cardiovasc. Res. 64 (2004) 125–131.
[9] M. Grohmann, The activity of the neuronal and extraneuronal catecholamine metabolizing enzymes of the perfused rat heart, Naunyn Schmiedebergs Arch. Pharmacol. 336 (1987) 139–147.
[10] M. Grohmann, U. Trendelenburg, The handling of five catecholamines by the extraneuronal *O*-methylating system of the rat heart, Naunyn Schmiedebergs Arch. Pharmacol. 329 (1985) 264–270.
[11] M. Inoue, K. Hifumi, K. Kurahashi, M. Fujiwara, Impairment of the extraneuronal *O*-methylating system of isoproterenol by stop-flow ischemia in the perfused rat heart, J. Pharmacol. Exp. Ther. 242 (1987) 1086–1089.
[12] L.L. Iversen, P.J. The uptake of catechol amines at high perfusion concentrations in the rat isolated heart: a novel catechol amine uptake process, Br. J. Pharmacol. 25 (1965) 18–33.
[13] W.R. Kaufman, B.I. Jugdutt, Left ventricular catecholamines during acute myocardial infarction in the dog, Can. J. Physiol. Pharmacol. 65 (1987) 172–178.
[14] T.W. Lameris, S. deZeeuw, G. Alberts, F. Boomsma, D.J. Duncker, P.D. Verdouw, A.J. Man in't Veld, A.H. van den Meiracker, Time course and mechanism of myocardial catecholamine release during transient ischemia in vivo, Circulation 101 (2000) 2645–2650.
[15] P. Mertes, K. El-Abbassi, Y. Jabpin, C. Michel, B. Beck, G. Pinelli, J. Carteaux, J. Villemot, C. Burlet, Consequences of coronary occlusion on changes in regional interstitial myocardial neuropeptide Y and norepinephrine concentrations, J. Mol. Cell. Cardiol. 28 (1996) 1995–2004.
[16] W.J. Penny, The deleterious effects of myocardial catecholamines on cellular electrophysiology and arrhythmias during ishaemia and reperfusion, Eur. Heart J. 5 (1984) 960–973.
[17] A. Schömig, T. Kurz, G. Richardt, E. Schömig, Neuronal sodium homeostatis and axoplasmic amine concentration determine calcium-independent noradrenaline release in normoxic and ischemic rat heart, Circ. Res. 63 (1988) 214–226.
[18] N. Tokunaga, T. Yamazaki, T. Akiyama, H. Mori, Detection of 3-methoxy-4-hydroxyphenylglycol in rabbit skeletal muscle microdialysate, J. Cnromatogr. B. 798 (2003) 163–166.
[19] U. Trendelenburg, H. Fleig, L.J. Bryan, H. Bönisch, The extraneuronal compartments for the distribution of isoprenaline in the rat heart, Naunyn Schmiedebergs Arch. Pharmacol. 324 (1983) 169–179.
[20] M. Valenza, E. Sarbinova, L. Packer, S. Khwaja, J. Catudioc, Nitecapone protects the Langendorff perfused heart against ischemia-reperfusion injury, Biochem. Mol. Biol. Int. 29 (1993) 443–449.
[21] A.P. Waldenström, A.C. Hjalmarson, L. Thornell, A possible role of noradrenaline in the development of myocardial infarction. An experimental study in the isolated rat heart, Am. Heart. J. 95 (1978) 43–51.
[22] T. Yamazaki, T. Akiyama, H. Kitagawa, T. Kawada, K. Sunagawa, Dialysate dihydroxyphenylglycol as a window for in situ axoplasmic norepinephrine disposition, Neurochem. Int. 38 (2001) 287–292.
[23] T. Yamazaki, T. Akiyama, T. Shindo, Routine high-performance liquid chromatographic determination of the myocardial interstitial norepinephrine, J. Chromatogr. B. 670 (1995) 328–331.

Acta Crystallographica Section F
Structural Biology and Crystallization Communications
ISSN 1744-3091

Youssef Ben Ammar,[a] Soichi Takeda,[b] Mitsuaki Sugawara,[c] Masashi Miyano,[c] Hidezo Mori[b] and Shigeo Wakabayashi[a]*

[a]Department of Molecular Physiology, National Cardiovascular Center Research Institute, Fujishiro-dai 5-7-1, Suita, Osaka 565-8565, Japan, [b]Department of Cardiac Physiology, National Cardiovascular Center Research Institute, Fujishiro-dai 5-7-1, Suita, Osaka 565-8565, Japan, and [c]Structural Biophysics Laboratory, RIKEN Harima Institute at SPring-8, Kouto, Mikazuki, Sayo, Hyogo 679-5148, Japan

Correspondence e-mail: wak@ri.ncvc.go.jp

Received 18 August 2005
Accepted 27 September 2005
Online 30 September 2005

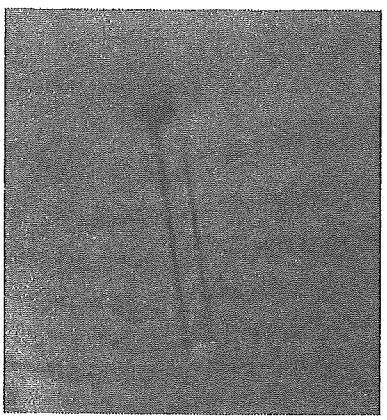

Crystallization and preliminary crystallographic analysis of the human calcineurin homologous protein CHP2 bound to the cytoplasmic region of the Na^+/H^+ exchanger NHE1

Calcineurin homologous protein (CHP) is a Ca^{2+}-binding protein that directly interacts with and regulates the activity of all plasma-membrane Na^+/H^+-exchanger (NHE) family members. In contrast to the ubiquitous isoform CHP1, CHP2 is highly expressed in cancer cells. To understand the regulatory mechanism of NHE1 by CHP2, the complex CHP2–NHE1 (amino acids 503–545) has been crystallized by the sitting-drop vapour-diffusion method using PEG 3350 as precipitant. The crystals diffract to 2.7 Å and belong to a tetragonal space group, with unit-cell parameters $a = b = 49.96$, $c = 103.20$ Å.

1. Introduction

The Na^+/H^+ exchangers (NHEs) are electroneutral transporters that catalyze the countertransport of Na^+ and H^+ through the plasma membrane and other intracellular organellar membranes in various animal species (Wakabayashi *et al.*, 1997; Orlowski & Grinstein, 2004). Nine different NHE isoforms (NHE1–NHE9) have been identified in mammalian tissues. Although they have been shown to exhibit similar membrane topology, these isoforms are thought to play different roles in various tissues (Counillon & Pouysségur, 2000; Orlowski & Grinstein, 2004). The isoform NHE1 is ubiquitously expressed in all tissues and cell types and plays a major role in maintaining intracellular pH and cell-volume homoeostasis (Putney *et al.*, 2002). The activity of NHE1 is controlled by various extrinsic factors, including growth factors, hormones and mechanical stimuli (Wakabayashi *et al.*, 1997; Counillon & Pouysségur, 2000; Orlowski & Grinstein, 2004). NHE1 is regulated by a variety of signalling molecules including calcineurin B homologous protein (CHP; Lin & Barber, 1996; Pang *et al.*, 2001) and Ca^{2+}/calmodulin (Bertrand *et al.*, 1994; Wakabayashi *et al.*, 1994). Despite intensive studies on NHE1 and its regulation, structural information is extremely limited, especially for the cytoplasmic C-terminal domain which contains most of the binding domains for the regulatory proteins.

CHP was initially identified as a protein (p22) involved in vesicular transport (Barroso *et al.*, 1996) and also as a molecule that interacts with NHE (Lin & Barber, 1996). CHP has also been reported to be involved in various cell functions, such as inhibition of calcineurin phosphatase activity (Lin *et al.*, 1999) and interaction with microtubules (Timm *et al.*, 1999), DRAK2 (death-associated protein kinase-related apoptosis-inducing protein kinase 2; Matsumoto *et al.*, 2001) and KIF1Bβ2 (kinesin family 1Bb2; Nakamura *et al.*, 2002). We have previously reported that CHP is an essential cofactor for supporting the physiological activity of the Na^+/H^+ exchanger by interacting with its juxtamembrane cytoplasmic domain (Pang *et al.*, 2001). Furthermore, we demonstrated that in contrast to the ubiquitous CHP1 isoform, CHP2 (61% amino-acid identity with CHP1) is highly expressed in malignantly transformed cells and may be involved in maintaining the high intracellular pH (pH_i) in cancer cells (Pang *et al.*, 2002). NHE1 mutants lacking the CHP-binding region (amino acids 515–530) exhibited low exchange activity (5–10% of the wild-type level; Pang *et al.*, 2001), suggesting that this region is essential for normal exchange activity of NHE1. This region with bound CHP would therefore function as a key structure maintaining the physiologically active conformation of NHE1 (Pang *et al.*, 2001).

Consequently, more detailed structural information including the crystal structure of CHP complexed with its binding domain is of great importance to reveal the mechanism by which CHP is involved in this important regulation pathway of NHE1.

Here, we report the first crystallization and preliminary crystallographic studies of the human CHP2 complexed with the C-terminal cytoplasmic region (amino acids 503–545) of NHE1. Hereafter, the protein complex is referred to as CHP2–NHE1-peptide.

2. Materials and methods

2.1. Protein expression and purification

Human CHP2 cDNA (GenBank accession No. AF146019) corresponding to amino-acid residues 1–196 cloned into pET11 vector (Novagen) as a fusion protein with a C-terminal His_6 tag was co-expressed in *Escherichia coli* (BL21-Star; Invitrogen) with the human cDNA encoding the cytoplasmic binding-domain region of NHE1 peptide cloned into pET24 vector (Novagen). Six histidine residues were inserted after Lys196 of CHP2, while a stop codon was incorporated just after the sequence coding for the NHE1 peptide to eliminate the His_6 tag from the vector. Using this coexpression system, as also described previously for CHP1 (Pang *et al.*, 2004), we were able to obtain CHP2 in a complex form with its binding domain of NHE1. Cells were cultured in 2×YT medium containing 100 μg ml^{-1} ampicillin and 100 μg ml^{-1} kanamycin at 310 K. At an optical density of 0.6 at 600 nm, protein expression was induced by the addition of IPTG to a final concentration of 1 m*M* and cells were grown overnight at 291 K. The cells were harvested and resuspended in PBS buffer containing 1 m*M* phenylmethylsulfonyl fluoride (PMSF) and disrupted by sonication at 277 K. After centrifugation at 277 K, the supernatant containing the complex CHP2–NHE1-peptide was applied onto an Ni–NTA agarose affinity column (Invitrogen) equilibrated with PBS buffer. The column was washed with buffer *A* (20 m*M* sodium phosphate, 500 m*M* NaCl and 2 *M* KCl pH 6.0), buffer *B* (20 m*M* sodium phosphate and 500 m*M* NaCl pH 4.7) and then buffer *C* (20 m*M* sodium phosphate and 500 m*M* NaCl pH 6.0). The adsorbed protein complex was eluted with buffer *C* containing 500 m*M* imidazole, dialyzed overnight against buffer *D* (20 m*M* Tris–HCl pH 8.5) and further purified using a DEAE-Sepharose column (HiTrap DEAE FF 5 ml; Amersham Biosciences) eluted with a gradient from 0 to 1 *M* NaCl in 20 m*M* Tris–HCl buffer pH 8.5. A final purification step was carried out using gel-filtration chromatography (Superdex 200; Amersham Bioscience). The gel-filtration column was eluted with a buffer solution containing 100 m*M* NaCl and 20 m*M* Tris–HCl pH 7.5. The fraction containing CHP2–NHE1-peptide was pooled, dialyzed against 20 m*M* Tris–HCl pH 7.5, concentrated (20–25 mg ml^{-1}) using Amicon Ultra (Millipore) and subjected to crystallization without removing the His_6 tag.

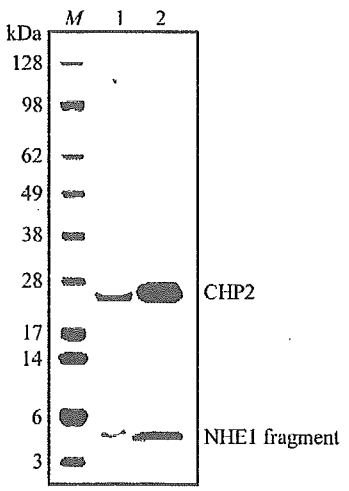

Figure 1
Polyacrylamide gel-electrophoresis pattern of the complex CHP2–NHE1-peptide. Crystals were collected and washed with the cryoprotectant solution. Collected crystals and 10 μg of the purified complex were applied to 4–12% gradient gel for lanes 1 and 2, respectively. Proteins were stained with Coomassie Brilliant Blue.

2.2. Crystallization

Preliminary screening of crystallization conditions was performed using various commercial kits (Hampton Research Crystal Screen kits, Emerald BioSystems Screen kits, Sigma–Aldrich Crystallization kits) and carried out using the sitting-drop vapour-diffusion method at 293, 287 and 277 K. 1 μl aliquots of protein-complex solution (20–25 mg ml^{-1}) were mixed with 1 μl reservoir solution to form the droplet, which was equilibrated against 100 μl reservoir solution. The initial screening, involving about 1440 individual trials, was unsuccessful. Additives from Hampton Research were used together with the above screening kits in a second trial involving about 4320 individual trials and very small and thin needle-shape crystals were finally obtained with a crystallization solution containing 200 m*M* ammonium acetate, 100 m*M* Bis-Tris pH 5.5, 25%(*w*/*v*) polyethylene glycol 3350 (PEG 3350) and 5 m*M* yttrium chloride as an additive at 277 K. Refinement of the crystallization conditions to 200 m*M* ammonium acetate, 100 m*M* Bis-Tris pH 5.5, 25%(*w*/*v*) PEG 3350 and 10 m*M* yttrium chloride at 293 K improved the size of the crystals. The resultant crystals are mostly in clusters, with the occasional appearance of single crystals. Single crystals or dissected parts from the clusters were used for data collection.

2.3. Crystallographic data collection

Prior to data collection, single crystals were soaked in a solution containing 200 m*M* ammonium acetate, 100 m*M* Bis-Tris pH 5.5, 35%(*w*/*v*) PEG 3350 and 10 m*M* yttrium chloride and flash-frozen under a nitrogen flow at 100 K. The crystals were evaluated in-house with Cu $K\alpha$ radiation (λ = 1.5418 Å) generated by an RA-Micro 7 rotating-anode X-ray generator with R-AXIS VII imaging-plate detector (Rigaku). High-resolution data sets were collected using an

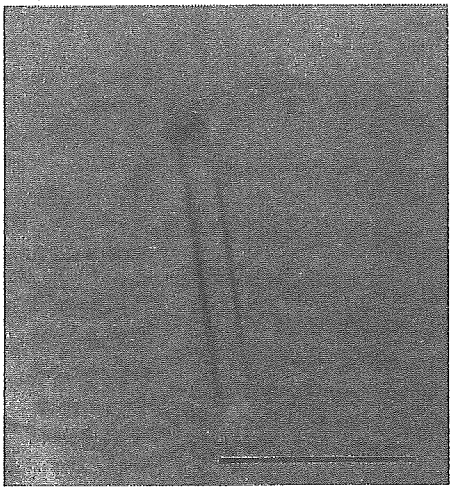

Figure 2
Crystal of human CHP2–NHE1-peptide as grown by the sitting-drop method. The scale bar indicates 0.1 mm.

Table 1
Data-collection statistics.

Values in parentheses are for the highest resolution shell (2.8–2.7 Å).

X-ray source	SPring-8 BL41XU
Space group	$P4_1$ or $P4_3$
Unit-cell parameters (Å, °)	$a = b = 49.96$, $c = 103.20$, $\alpha = \beta = \gamma = 90$
Wavelength (Å)	1.0000
Resolution range (Å)	50.00–2.70 (2.80–2.70)
Total reflections	26984
Unique reflections	6807
$R_{\rm merge}$† (%)	4.8 (25.1)
Completeness (%)	97.3 (83.1)
$\langle I/\sigma(I)\rangle$	17.3 (4.5)
Redundancy	4.0 (3.1)
Crystal mosaicity (°)	0.458

† $R_{\rm merge} = \sum_{hkl}\sum_i |I_i(hkl) - \langle I(hkl)\rangle| / \sum_{hkl}\sum_i I_i(hkl)$, where $I_i(hkl)$ is the ith intensity measurement of reflection hkl and $\langle I(hkl)\rangle$ is its average.

ADSC Quantum 315 CCD detector installed on the BL41XU beamline at SPring-8. The data collection was performed at a wavelength of 1.000 Å over a total range of 180°, with individual frames of 1° and an exposure time of 4 s. The crystal-to-detector distance was 350 mm. The collected images were processed using *HKL*2000 (Otwinowski & Minor, 1997).

3. Results and discussion

CHP is an important regulatory factor that maintains the physiologically active conformation of NHE1. In this study, in order to clarify the regulatory mechanism of NHE1 by CHP, we coexpressed CHP2 and its binding domain in NHE1 (amino acids 503–545) in *E. coli* and crystallized the complex. Firstly, we confirmed that the purified complex CHP2–NHE1-peptide was retained as a single peak on gel-filtration chromatography, indicating that the stable complex exists as a monomer (M_r = 28 000) in solution. In addition, using a 4–12% polyacrylamide gradient gel we confirmed that the purity of the complex is suitable for crystallization assay and that the purified sample contained equimolar amounts (1:1 molar ratio) of CHP2 and NHE1-peptide (Fig. 1).

Crystals suitable for X-ray crystallographic analysis were obtained within 2–3 d at 293 K using the sitting-drop vapour-diffusion method (Fig. 2). A previous attempt to collect crystallographic data at beamline BL44B2 (SPring-8) gave a maximum resolution of 3.0 Å owing to the small size of crystals. To obtain higher resolution data, we used the undulator beamline BL41XU. Crystals diffracted to 2.5 Å resolution along the c axis of the crystal, but the data set was only qualitatively useful to 2.7 Å because of anisotropic diffraction.

The tetragonal crystal of CHP2–NHE1-peptide was determined to be $P4_1$ or $P4_3$, with unit-cell parameters $a = b = 49.96$, $c = 103.20$ Å. Assuming the presence of one CHP2–NHE1-peptide complex molecule in the asymmetric unit, the Matthews coefficient V_M was calculated to be 2.5 Å^3 Da^{-1}, indicating a solvent content of approximately 49.5% in the unit cell. These values are within the typical range for protein crystals (Matthews, 1968).

The native data set has 6807 unique reflections, giving a data-set completeness of 97.3% in the resolution range 50.0–2.7 Å, with an $R(I)_{\rm merge}$ of 4.8% (Table 1). Although CHP2 shows about 36% sequence identity with human CNB (PDB code 1aui; Kissinger *et al.*, 1995), molecular replacement using CNB as a search model with *MOLREP* (Vagin & Teplyakov, 1997) was unsuccessful. Further crystallization refinement and structural analysis by multi-wavelength anomalous dispersion methods using selenomethionine and also taking advantage of the presence of yttrium as an additive are in progress.

We thank the staff at beamlines BL44B2 and BL41XU, SPring-8 for data-collection support and Dr Tianxiang Pang for initial participation in this study. This work was supported by grant Nano-001 for Research on Advanced Medical Technology from the Ministry of Health, Labour and Welfare of Japan and Grant-in-Aid for Priority Areas 13142210 for Scientific Research from the Ministry of Education, Science and Culture of Japan. YBA was supported by a Japan Society for the Promotion of Science (JSPS) Postdoctoral Fellowship.

References

Barroso, M. R., Bernd, K. K., DeWitt, N. D., Chang, A., Mills, K. & Sztul, E. S. (1996). *J. Biol. Chem.* **271**, 10183–10187.
Bertrand, B., Wakabayashi, S., Ikeda, T., Pouysségur, J. & Shigekawa, M. (1994). *J. Biol. Chem.* **269**, 13703–13709.
Counillon, L. & Pouysségur, J. (2000). *J. Biol. Chem.* **275**, 1–4.
Kissinger, C. R., Parge, H. E., Knighton, D. R., Lewis, C. T., Pelletier, L. A., Tempczyk, A., Kalish, V. J., Tucker, K. D., Showalter, R. E., Moomaw, E. W., Gastinel, L. N., Habuka, N., Chen, X., Maldonado, F., Barker, J. E., Bacquet, R. & Villafranca, J. E. (1995). *Nature (London)*, **378**, 641–644.
Lin, X. & Barber, D. L. (1996). *Proc. Natl Acad. Sci. USA*, **93**, 12631–12636.
Lin, X., Sikkink, R. A., Rusnak, F. & Barber, D. L. (1999). *J. Biol. Chem.* **274**, 36125–36131.
Matsumoto, M., Miyake, Y., Nagita, M., Inoue, H., Shitakubo, D., Takemoto, K., Ohtsuka, C., Murakami, H., Nakamura, N. & Kanazawa, H. (2001). *J. Biochem.* **130**, 217–225.
Matthews, B. W. (1968). *J. Mol. Biol.* **33**, 491–497.
Nakamura, N., Miyake, Y., Matsushita, M., Tanaka, S., Inoue, H. & Kanazawa, H. (2002). *J. Biochem.* **132**, 483–491.
Orlowski, J. & Grinstein, S. (2004). *Pflugers Arch.* **447**, 549–565.
Otwinowski, Z. & Minor, W. (1997). *Methods Enzymol.* **276**, 307–326.
Pang, T., Hisamitsu, T., Mori, H., Shigekawa, M. & Wakabayashi, S. (2004). *Biochemistry*, **43**, 3628–3636.
Pang, T., Su, X., Wakabayashi, S. & Shigekawa, M. (2001). *J. Biol. Chem.* **276**, 17367–17372.
Pang, T., Wakabayashi, S. & Shigekawa, M. (2002). *J. Biol. Chem.* **277**, 43771–43777.
Putney, L. K., Denker, S. P. & Barber, D. L. (2002). *Annu. Rev. Pharmacol. Toxicol.* **42**, 527–552.
Timm, S., Titus, B., Bernd, K. & Barroso, M. (1999). *Mol. Biol. Cell*, **10**, 3473–3488.
Vagin, A. A. & Teplyakov, A. (1997). *J. Appl. Cryst.* **30**, 1022–1025.
Wakabayashi, S., Bertrand, B., Ikeda, T., Pouysségur, J. & Shigekawa, M. (1994). *J. Biol. Chem.* **269**, 13710–13715.
Wakabayashi, S., Shigekawa, M. & Pouyssegur, J. (1997). *Physiol. Rev.* **77**, 51–74.

原子核研究
Vol. 49 No. 5
研究会報告

Conventional enhanced K-edge angiography utilizing cerium x-ray generator

Eiichi Sato[a], Akira Yamadera[b], Toshio Ichimaru[b], Etsuro Tanaka[c], Hidezo Mori[d], Toshiaki Kawai[e], Takashi Inoue[f], Akira Ogawa[f], Shigehiro Sato[g], Kazuyoshi Takayama[h] and Hideaki Ido[i]

[a] Department of Physics, Iwate Medical University, 3-16-1 Honchodori, Morioka 020-0015, Japan

[b] Department of Radiological Technology, School of Health Sciences, Hirosaki University, 66-1 Honcho, Hirosaki 036-8564, Japan

[c] Department of Nutritional Science, Faculty of Applied Bio-science, Tokyo University of Agriculture, 1-1-1 Sakuragaoka, Setagaya-ku 156-8502, Japan

[d] Department of Cardiac Physiology, National Cardiovascular Center Research Institute, 5-7-1 Fujishirodai, Suita, Osaka 565-8565, Japan

[e] Electron Tube Division #2, Hamamatsu Photonics K. K., 314-5 Shimokanzo, Toyooka Village, Iwata-gun 438-0193, Japan

[f] Department of Neurosurgery, School of Medicine, Iwate Medical University, 19-1 Uchimaru, Morioka 020-8505, Japan

[g] Department of Microbiology, School of Medicine, Iwate Medical University, 19-1 Uchimaru, Morioka 020-8505, Japan

[h] Shock Wave Research Center, Institute of Fluid Science, Tohoku University, 2-1-1 Katahira, Sendai 980-8577, Japan

[i] Department of Applied Physics and Informatics, Faculty of Engineering, Tohoku Gakuin University, 1-13-1 Chuo, Tagajo 985-8537, Japan

Abstract

The cerium-target x-ray tube is useful in order to perform cone-beam K-edge angiography because Kα rays from the cerium target are absorbed effectively by iodine-based contrast media. The maximum tube voltage and current were 65 kV and 0.40 mA, respectively, and the focal-spot sizes were approximately 1×1 mm. Sharp cerium Kα lines were left using a barium sulfate filter, and the x-ray

intensity was 16.8 μGy/s at 1.0 m from the source with a tube voltage of 60 kV and a current of 0.40 mA. Angiography was performed using iodine-based microspheres 15 μm in diameter. In angiography of non-living animals, we observed fine blood vessels of 100 μm or less.

1. Introduction

Synchrotrons generate monochromatic parallel x-ray beams using single crystals. These beams with photon energies of approximately 35 keV have been employed to perform enhanced K-edge angiography,[1-3] since the beams are absorbed effectively by iodine-based contrast media.

In order to perform high-speed medical radiography, although several different flash x-ray generators[4-9] utilizing cold-cathode tubes have been developed, plasma flash x-ray generators[10-13] are useful to produce quasi-monochromatic x rays without using a K-edge filter. Therefore, we have performed a demonstration of cone-beam K-edge angiography[14] utilizing a cerium plasma generator, since K-series characteristic x rays from the cerium target are absorbed effectively by iodine. Recently, we have developed a steady-state x-ray generator utilizing a cerium-target tube, and have demonstrated enhanced K-edge angiography utilizing a barium sulfate filter.[15] In this research, Kα lines (34.6 keV) were left by absorbing Kβ lines (39.2 keV).

In the present research, we describe a preliminary study on cone-beam K-edge angiography achieved with cerium Kα rays using a barium sulfate filter.

2. Generator

Figure 1 shows the block diagram of the x-ray generator, which consists of a main controller, a cerium-target x-ray tube unit with a Cockcroft-Walton circuit and an insulation transformer, and a personal computer. The tube voltage, the current, and the exposure time can be controlled by both the controller and the computer. The main circuit for producing x rays is illustrated in Fig. 2, and employs the Cockcroft-Walton circuit in order to decrease the dimensions of the tube unit. In the x-ray tube, the negative high-voltage is applied to the cathode electrode, and the anode (target) is connected to the tube unit case (ground potential) to cool the anode and the target effectively. The filament heating current is supplied by an AC power supply in the controller in conjunction with an insulation transformer. In this experiment, the tube voltage applied was from 45 to 65 kV, and the tube current was regulated to within 0.40 mA (maximum current) by the filament temperature. The exposure time is controlled in order to obtain optimum x-ray intensity. Monochromatic Kα lines were left using a 5-mm-thick barium sulfate filter in which barium sulfate powder was mixed with polymethyl methacrylate (PMMA) resin, since both the bremsstrahlung and the Kβ rays were absorbed effectively by the filter. In designing the filter, the surface density of the barium sulfate powder is important, since the x rays are absorbed effectively by the powder as compared with the PMMA resin. In this case, the density was approximately 10 mg/cm^2.

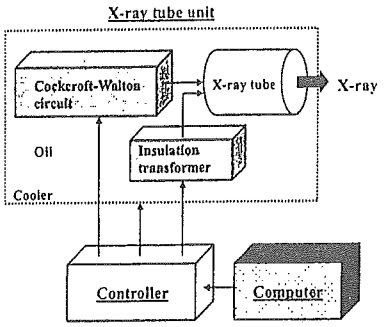

Fig. 1: Block diagram of compact x-ray generator with cerium-target tube.

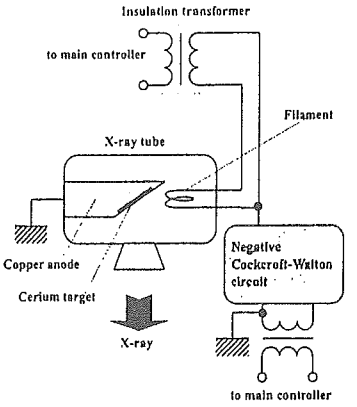

Fig. 2: Main circuit of x-ray generator.

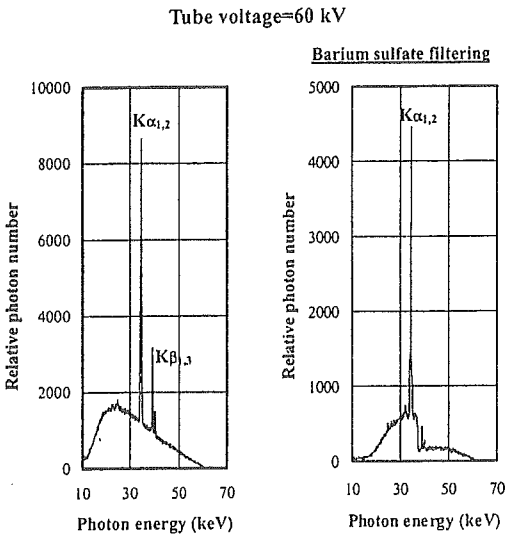

Fig. 3: X-ray spectra measured using germanium detector and filter.

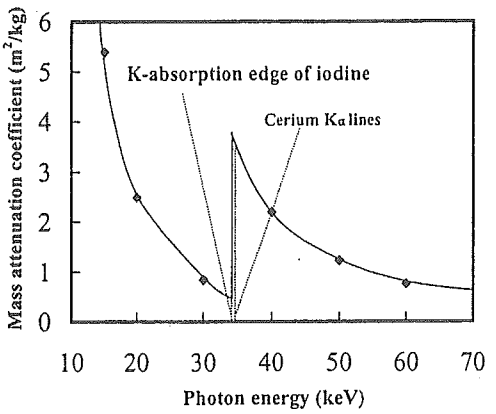

Fig. 4: Mass attenuation coefficients of iodine, and average photon energy of cerium Kα lines.

3. Characteristics

The x-ray intensity rate was measured by a Victoreen 660 ionization chamber at 1.0 m from the x-ray source. At a constant tube current of 0.40 mA, the x-ray intensity increased when the tube voltage was increased. In this measurement, the intensity with a tube voltage of 60 kV and a current of 0.40 mA was 16.8 μGy/s with errors of less than 0.2%.

In order to measure images of the x-ray source, we employed a pinhole camera with a hole diameter of 50 μm in conjunction with a Computed Radiography (CR) system[16] with a sampling pitch of 87.5 μm. When the tube voltage was increased, spot dimensions increased slightly and had values of

approximately 1×1 mm.

In order to measure x-ray spectra, we employed a germanium detector (GLP-10180/07-P, Ortec Inc.) (Fig. 3). When the tube voltage was increased, the Kα intensity substantially increased, and both the maximum photon energy and the intensities of bremsstrahlung x rays increased.

4. Angiography

Figure 4 shows the mass attenuation coefficients of iodine at the selected energies; the coefficient curve is discontinuous at the iodine K-edge. The average photon energy of the cerium Kα lines is shown just above the iodine K-edge. Cerium is a rare earth element and has a high reactivity; however, the average photon energies of Kα is 34.6 keV, and iodine contrast mediums with a K-absorption edge of 33.2 keV absorb the lines easily. Therefore, blood vessels were observed with high contrasts.

The angiography was performed using the CR system (Konica Regius 150), iodine microspheres of 15 μm in diameter, and the filter. The distance (between the x-ray source and the imaging plate) was 1.5 m, and the tube voltage was 60 kV. Figure 5 shows angiograms of an extracted dog heart. Because the size of the dog heart is almost the same as human heart, human coronary arteries can be observed.

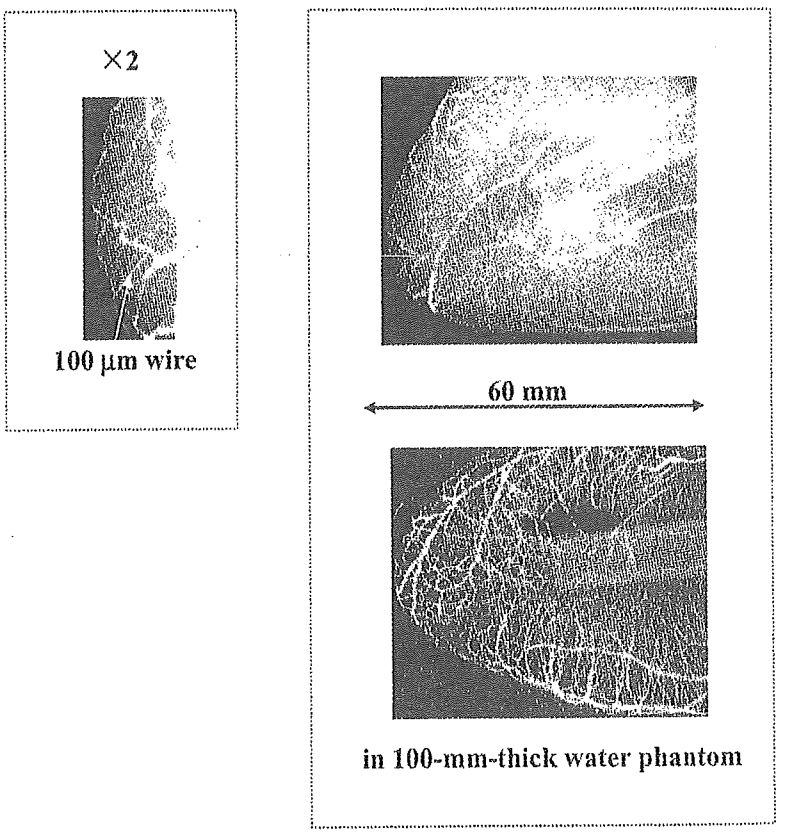

Fig. 5: Angiogram of extracted dog heart using iodine microspheres.

5. Discussion and Conclusions

In summary, we developed a new x-ray generator with a cerium-target tube and succeeded in producing cerium Kα lines, which can be absorbed easily by iodine-based contrast media. Both the characteristic and bremsstrahlung x-ray intensities increased with increases in the tube voltage, and Kβ lines were absorbed effectively by the barium sulfate filter.

In this preliminary experiment, although the maximum tube voltage and current were 65 kV and 0.40 mA, respectively, the voltage and current could be increased. Subsequently, the generator produced maximum number of Kα photons was approximately 3×10^7 photons/cm^2·s at 1.0 m from the source, and the photon count rate can be increased easily by improving the target.

Acknowledgment

This work was supported by Grants-in-Aid for Scientific Research (13470154, 13877114, and 16591222) and Advanced Medical Scientific Research from MECSST, Health and Labor Sciences Research Grants (RAMT-nano-001, RHGTEFB-genome-005 and RHGTEFB-saisei-003), Grants from Keiryo Research Foundation, The Promotion and Mutual Aid Corporation for Private Schools of Japan, Japan Science and Technology Agency (JST), and New Energy and Industrial Technology Development Organization (NEDO, Industrial Technology Research Grant Program in '03).

References

1. A. C. Thompson, H. D. Zeman, G. S. Brown, J. Morrison, P. Reiser, V. Padmanabahn, L. Ong, S. Green, J. Giacomini, H. Gordon and E. Rubenstein, "First operation of the medical research facility at the NSLS for coronary angiography," *Rev. Sci. Instrum.*, **63**, 625-628, 1992.

2. H. Mori, K. Hyodo, E. Tanaka, M. U. Mohammed, A. Yamakawa, Y. Shinozaki, H. Nakazawa, Y. Tanaka, T. Sekka, Y. Iwata, S. Honda, K. Umetani, H. Ueki, T. Yokoyama, K. Tanioka, M. Kubota, H. Hosaka, N. Ishizawa and M. Ando, "Small-vessel radiography in situ with monochromatic synchrotoron radiation," *Radiology*, **201**, 173-177, 1996.

3. K. Hyodo, M. Ando, Y. Oku, S. Yamamoto, T. Takeda, Y. Itai, S. Ohtsuka, Y. Sugishita and J. Tada, "Development of a two-dimensional imaging system for clinical applications of intravenous coronary angiography using intense synchrotron radiation produced by a multipole wiggler," *J. Synchrotron Rad.*, **5**, 1123-1126, 1998.

4. E. Sato, H. Isobe and F. Hoshino, "High intensity flash x-ray apparatus for biomedical radiography," *Rev. Sci. Instrum.*, **57**, 1399-1408, 1986.

5. E. Sato, S. Kimura, S. Kawasaki, H. Isobe, K. Takahashi, Y. Tamakawa and T. Yanagisawa, "Repetitive flash x-ray generator utilizing a simple diode with a new type of energy-selective function," *Rev. Sci. Instrum.*, **61**, 2343-2348, 1990.

6. A. Shikoda, E. Sato, M. Sagae, T. Oizumi, Y. Tamakawa and T. Yanagisawa, "Repetitive flash x-ray

generator having a high-durability diode driven by a two-cable-type line pulser," *Rev. Sci. Instrum.*, **65**, 850-856, 1994.

7. E. Sato, K. Takahashi, M. Sagae, S. Kimura, T. Oizumi, Y. Hayasi, Y. Tamakawa and T. Yanagisawa, "Sub-kilohertz flash x-ray generator utilizing a glass-enclosed cold-cathode triode," *Med. & Biol. Eng. & Comput.*, **32**, 289-294, 1994.

8. E. Sato, M. Sagae, E. Tanaka, Y. Hayasi, R. Germer, H. Mori, T. Kawai, T. Ichimaru, S. Sato, K. Takayama and H. Ido, "Quasi-monochromatic flash x-ray generator utilizing a disk-cathode molybdenum tube," *Jpn. J. Appl. Phys.*, **43**, 7324-7328, 2004.

9. E. Sato, E. Tanaka, H. Mori, T. Kawai, T. Ichimaru, S. Sato, K. Takayama and H. Ido, "Compact monochromatic flash x-ray generator utilizing a disk-cathode molybdenum tube," *Med. Phys.*, **32**, 49-54, 2005.

10. E. Sato, Y. Hayasi, R. Germer, E. Tanaka, H. Mori, T. Kawai, H. Obara, T. Ichimaru, K. Takayama and H. Ido, "Irradiation of intense characteristic x-rays from weakly ionized linear molybdenum plasma," *Jpn. J. Med. Phys.*, **23**, 123-131, 2003.

11. E. Sato, Y. Hayasi, R. Germer, E. Tanaka, H. Mori, T. Kawai, T. Ichimaru, K. Takayama and H. Ido, "Quasi-monochromatic flash x-ray generator utilizing weakly ionized linear copper plasma," *Rev. Sci. Instrum.*, **74**, 5236-5240, 2003.

12. E. Sato, R. Germer, Y. Hayasi, Y. Koorikawa, K. Murakami, E. Tanaka, H. Mori, T. Kawai, T. Ichimaru, F. Obata, K. Takahashi, S. Sato, K. Takayama and H. Ido, "Weakly ionized plasma flash x-ray generator and its distinctive characteristics," *SPIE*, **5196**, 383-392, 2003.

13. E. Sato, Y. Hayasi, R. Germer, E. Tanaka, H. Mori, T. Kawai, T. Ichimaru, S. Sato, K. Takayama and H. Ido, "Sharp characteristic x-ray irradiation from weakly ionized linear plasma," *J. Electron Spectrosc. Related Phenom.*, **137-140**, 713-720, 2004.

14. E. Sato, R. Germer, Y. Hayasi, K. Murakami, Y. Koorikawa, E. Tanaka, H. Mori, T. Kawai, T. Ichimaru, F. Obata, K. Takahashi, S. Sato, K. Takayama and H. Ido, "Weakly ionized cerium plasma radiography," *SPIE*, **5210**, 12-21, 2003.

15. E. Sato, E. Tanaka, H. Mori, T. Kawai, T. Ichimaru, S. Sato, K. Takayama and H. Ido, "Demonstration of enhanced K-edge angiography using a cerium target x-ray generator," *Med. Phys.*, **31**, 3017-3021, 2004.

16. E. Sato, K. Sato and Y. Tamakawa, "Film-less computed radiography system for high-speed imaging," *Ann. Rep. Iwate Med. Univ. Sch. Lib. Arts and Sci.*, **35**, 13-23, 2000.

原子核研究
Vol. 49 No. 5
研究会報告

Preliminary experiment for producing higher harmonic x rays utilizing copper plasma triode

Eiichi Sato[a], Etsuro Tanaka[b], Hidezo Mori[c], Toshiaki Kawai[d], Takashi Inoue[e], Akira Ogawa[e], Shigehiro Sato[f], Kazuyoshi Takayama[g] and Hideaki Ido[h]

[a] Department of Physics, Iwate Medical University, 3-16-1 Honchodori, Morioka 020-0015, Japan

[b] Department of Nutritional Science, Faculty of Applied Bio-science, Tokyo University of Agriculture, 1-1-1 Sakuragaoka, Setagaya-ku 156-8502, Japan

[c] Department of Cardiac Physiology, National Cardiovascular Center Research Institute, 5-7-1 Fujishirodai, Suita, Osaka 565-8565, Japan

[d] Electron Tube Division #2, Hamamatsu Photonics K. K., 314-5 Shimokanzo, Toyooka Village, Iwata-gun 438-0193, Japan

[e] Department of Neurosurgery, School of Medicine, Iwate Medical University, 19-1 Uchimaru, Morioka 020-8505, Japan

[f] Department of Microbiology, School of Medicine, Iwate Medical University, 19-1 Uchimaru, Morioka 020-8505, Japan

[g] Shock Wave Research Center, Institute of Fluid Science, Tohoku University, 2-1-1 Katahira, Sendai 980-8577, Japan

[h] Department of Applied Physics and Informatics, Faculty of Engineering, Tohoku Gakuin University, 1-13-1 Chuo, Tagajo 985-8537, Japan

Abstract

In the plasma flash x-ray generator, a 200 nF condenser is charged up to 50 kV by a power supply, and flash x rays are produced by the discharging. The x-ray tube is a demountable triode with a trigger electrode, and the turbomolecular pump evacuates air from the tube with a pressure of approximately 1 mPa. Target evaporation leads to the formation of weakly ionized linear plasma, consisting of copper ions and electrons, around the fine target, and intense Kα lines are left using a 10-μm-thick nickel filter. At a charging voltage of 50 kV, the maximum tube voltage was almost equal to the charging voltage of the main condenser, and the peak current was about 15 kA. The K-series characteristic x

rays were clean and intense, and higher harmonic x rays were observed. The x-ray pulse widths were approximately 700 ns, and the time-integrated x-ray intensity had a value of approximately 20 μC/kg at 1.0 m from the x-ray source with a charging voltage of 50 kV.

1. Introduction

Recently, soft x-ray lasers have been produced by a gas-discharge capillary,[1-4] and the laser pulse energy substantially increased in proportion to the capillary length. However, it is difficult to increase the laser photon energy to 10 keV or beyond. Because there are no x-ray resonators in the high-photon-energy region, new methods for increasing coherence will be desired in the future.

To perform high-speed soft radiography, several different flash x-ray generators[5-10] have been developed corresponding to specific objectives. Subsequently, we have developed a compact flash x-ray generator utilizing a disk-cathode demountable diode,[11,12] and have performed a preliminary experiment for producing clean characteristic x rays utilizing angle dependence of bremsstrahlung x rays.

With recent advances in high-voltage pulse technology, several different plasma flash x-ray generators have been developed corresponding to specific radiographic objectives, and a major goal in our research is the development of an intense and sharp monochromatic x-ray generator that can impact applications with biomedical radiography.

In this paper, we describe a plasma flash x-ray generator[13-15] utilizing a rod-target radiation tube, used to perform a preliminary experiment for generating intense and clean K-series characteristic x rays and their higher harmonic x rays by forming a linear copper plasma cloud around a fine target.

2. Generator

Figure 1 shows a block diagram of the high-intensity plasma flash x-ray generator. This generator consists of the following essential components: a high-voltage power supply, a high-voltage condenser with a capacity of approximately 200 nF, a turbomolecular pump, a krytron pulse generator as a trigger device, and a flash x-ray tube. The high-voltage main condenser is charged to 50 kV by the power supply, and electric charges in the condenser are discharged to the tube after triggering the cathode electrode with the trigger device. The plasma flash x rays are then produced.

The x-ray tube is a demountable cold-cathode triode that is connected to the turbomolecular pump with a pressure of approximately 1 mPa. This tube consists of the following major parts: a hollow cylindrical carbon cathode with a bore diameter of 10.0 mm, a brass focusing electrode, a trigger electrode made from copper wire, a stainless steel vacuum chamber, a nylon insulator, a polyethylene terephthalate (Mylar) x-ray window 0.25 mm in thickness, and a rod-shaped copper target 3.0 mm in diameter with a tip angle of 60°. The distance between the target and cathode electrodes is

approximately 20 mm, and the trigger electrode is set in the cathode electrode. As electron beams from the cathode electrode are roughly converged to the target by the focusing electrode, evaporation leads to the formation of a weakly ionized linear plasma, consisting of copper ions and electrons, around the fine target.

In the linear plasma, bremsstrahlung photons with energies higher than the K-absorption edge are effectively absorbed and are converted into fluorescent x rays (Fig. 2). The plasma then transmits the fluorescent rays easily, and bremsstrahlung rays with energies lower than the K-edge are also absorbed by the plasma. In addition, because bremsstrahlung rays are not emitted in the opposite direction to that of electron acceleration, intense characteristic x rays are generated from the plasma-axial direction.

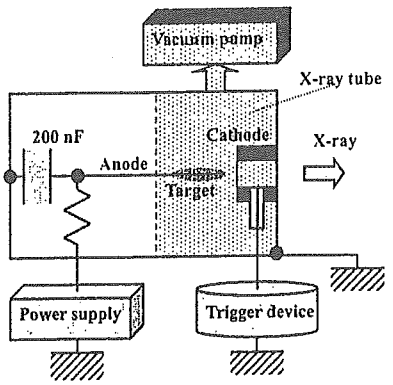

Fig. 1: Block diagram including electric circuit of plasma flash x-ray generator.

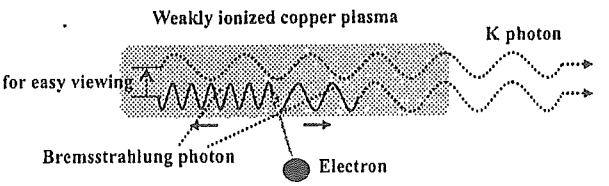

Fig. 2: K-photon irradiation from plasma.

3. Characteristics

Tube voltage and current were measured by a high-voltage divider with an input impedance of 1 GΩ and a current transformer, respectively. At a charging voltage of 50 kV, the maximum tube voltage was almost equal to the charging voltage of the main condenser, and the maximum tube current was approximately 15 kA.

X-ray output pulse was detected by a combination of a plastic scintillator and a photomultiplier using a 10-μm-thick nickel filter. The x-ray pulse height substantially increased with corresponding increases in the charging voltage. The x-ray pulse widths were about 700 ns, and the time-integrated x-ray intensity per pulse measured by a thermoluminescence dosimeter (Kyokko TLD Reader 1500 utilizing MSO-S elements without energy compensation) had a value of about 20 μC/kg at 1.0 m from the x-ray source with a charging voltage of 50 kV.

X-ray spectra from the plasma source were measured by a transmission-type spectrometer with a lithium fluoride curved crystal 0.5 mm in thickness. The spectra were taken by a computed radiography (CR) system[16] (Konica Regius 150) with a wide dynamic range, using the filter, and

relative x-ray intensity was calculated from Dicom digital data. Figure 3 shows measured spectra from the copper target with a charging voltage of 50 kV. In fact, we observed clean K lines such as lasers, and Kα lines were left by absorbing Kβ lines using the filter. The characteristic x-ray intensity substantially increased with corresponding increases in the charging voltage, and higher harmonic x rays were observed.

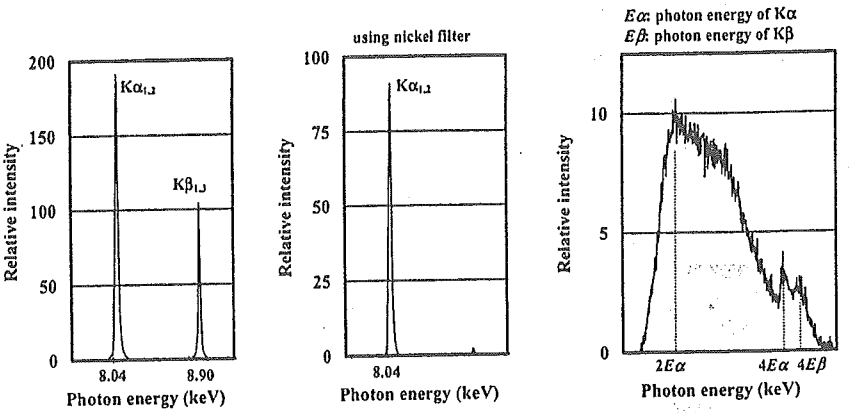

Fig. 3: X-ray spectra from weakly ionized copper plasma at indicated conditions.

4. Radiography

The plasma radiography was performed by the CR system using the filter. The charging voltage and the distance between the x-ray source and imaging plate were 50 kV and 1.2 m, respectively.

Firstly, an image of plastic bullets falling into a polypropylene beaker from a plastic test tube is shown in Fig. 4. Because the x-ray duration was about 1 μs, the stop-motion image of bullets could be obtained. Figure 5 shows an angiogram of a rabbit ear; iodine-based microspheres of 15 μm in diameter were used, and fine blood vessels of about 50 μm were visible.

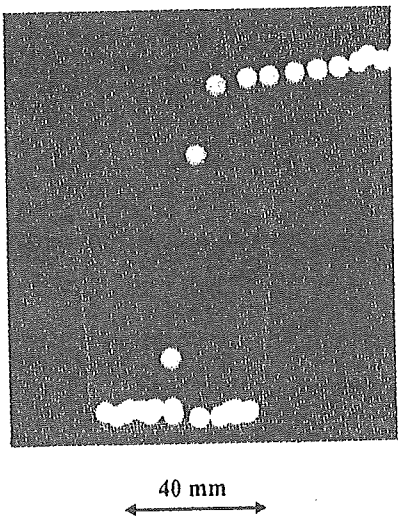

Fig. 4: Radiogram of water falling into polypropylene beaker from plastic test tube.

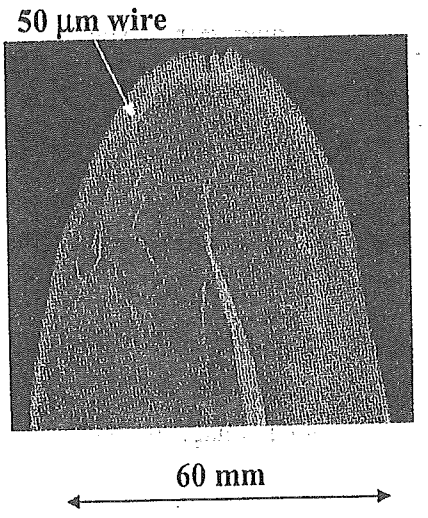

Fig. 5: Angiograms of rabbit ear.

5. Discussion and Conclusions

Concerning the spectrum measurement, we obtained fairly intense and clean K lines from a weakly ionized linear plasma x-ray source, and Kα lines were left by absorbing Kβ lines using the nickel filter. In particular, the higher harmonic x rays were produced from the plasma. Assuming that the harmonic rays are produced by the x-ray resonation (Fig. 6), the estimated spectra are shown in Fig. 7. In cases where a copper target is employed, fractional harmonic x rays are absorbed by an x-ray window and air.

In this research, we obtained sufficient characteristic x-ray intensity per pulse for CR radiography, and the generator produced number of characteristic Kα photons was approximately 5×10^7 photons/cm^2 at 1.0 m per pulse. In addition, since the photon energy of characteristic x rays can be controlled by changing the target elements, various quasi-monochromatic high-speed radiographies, such as high-contrast angiography and mammography, will be possible.

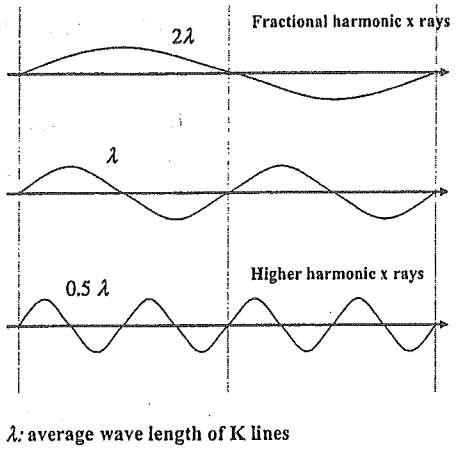

Fig. 6: X-ray resonation without using resonator.

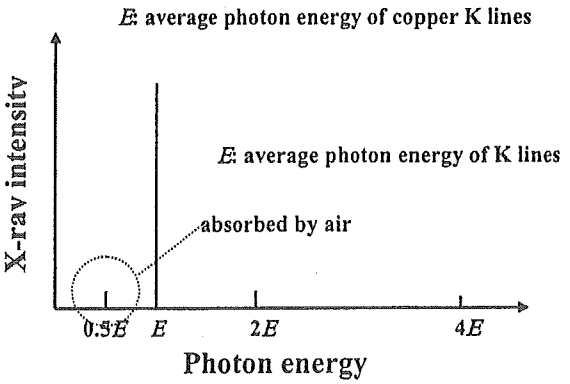

Fig. 7: Estimated x-ray spectra under resonation.

Acknowledgment

This work was supported by Grants-in-Aid for Scientific Research (13470154, 13877114, and 16591222) and Advanced Medical Scientific Research from MECSST, Health and Labor Sciences Research Grants(RAMT-nano-001, RHGTEFB-genome-005 and RHGTEFB-saisei-003), Grants from Keiryo Research Foundation, The Promotion and Mutual Aid Corporation for Private Schools of Japan, Japan Science and Technology Agency (JST), and New Energy and Industrial Technology Development Organization (NEDO, Industrial Technology Research Grant Program in '03).

References

1. J.J. Rocca, V. Shlyaptsev, F.G. Tomasel, O.D. Cortazar, D. Hartshorn and J.L.A. Chilla, "Demonstration of a discharge pumped table-top soft x-ray laser," *Proc. Phys. Lev. Lett.*, 73,